International Journal of Thermal Sciences 187 (2023) 108164

Contents lists available at ScienceDirect

International Journal of Thermal Sciences

journal homepage: www.elsevier.com/locate/ijts

Solid and gas thermal conductivity models improvement and validation in various porous insulation materials

Som S. Shrestha [a,**], Janak Tiwari [b], Amit Rai [c], Diana E. Hun [a], Daniel Howard [a], Andre O. Desjarlais [a], Mathieu Francoeur [d], Tianli Feng [b,*]

[a] Buildings and Transportation Science Division, Oak Ridge National Laboratory, Oak Ridge, TN, 37831, USA
[b] Department of Mechanical Engineering, University of Utah, Salt Lake City, UT, 84112, USA
[c] Department of Physics, University of Dayton, Dayton, OH, 45469, USA
[d] Department of Mechanical Engineering, McGill University, Montréal, QC, H3A 0C3, Canada

ARTICLE INFO

Keywords:
Thermal conductivity
Thermal insulation materials
Effective medium theory
Knudsen effect
Radiative heat transfer

ABSTRACT

In the past few decades, significant efforts have been made to improve the theoretical understanding of thermal transport mechanisms in thermal insulation materials and push the thermal conductivity's lower limits. However, most works focused singularly on specific types of materials, and the models used for thermal conductivity predictions are diverse - a model that fits one material might not fit others. Here, we improve and unify the gas and solid thermal conductivity models for porous materials. Through experimental characterization of several different materials as well as literature data for other materials, these models are validated. We have also found that the pressure-dependent gas thermal conductivity of most materials can be well fitted by using one or two pore sizes without using a complex pore size distribution. With the refined models, we decompose the effective thermal conductivity of several thermal insulation materials into gas, solid, and radiation contributions. For cellular (polystyrene and polyurethane) foams, the relative contributions from air, solid, and radiation are 58–75%, 3–11%, 16–38%, respectively. For granular porous materials (polyurethane and silica in this work), the contributions from air, solid, and radiation are 45–66%, 34–46%, and 0–8%, respectively. This work is expected to provide guidance on the design and optimization of the next generation of thermal insulation materials, for example, through the effort of reducing gas conduction and radiation in foams and suppressing gas and solid conduction in aerogels.

1. Introduction

Thermal insulation materials with ultra-low effective thermal conductivity are critical for a variety of applications, including building envelopes [1–3], pipelines for oil, water, and natural gas transportation [4], aircraft and reentry spacecraft [5], engine and exhaust systems in automobiles [6], refrigerators, freezers, and tanks [7,8], and cold chain systems for vaccines [9]. For example, buildings are the largest energy consumption sector in the United States [10] and the European Union [11], responsible for about 40% of the total annual primary energy use. Unwanted heat flows through building envelopes (walls, roofs, and foundations) are responsible for 7.7×10^{18} J (7.3 quads) of energy consumption in 2010, and the number is projected to be 7.17×10^{18} J (6.8 quads) in 2035 [12]. Developing high-performance thermal insulation materials will decrease these unwanted heat flows, and therefore save energy, reduce greenhouse gas emissions, improve energy security, and lessen dependency on fossil fuels. The potential for energy savings in 2030 in U.S. residential buildings by using thermal insulation materials in walls with thermal resistivities of 42, 56, and 83 m K/W (R-6, R-8, and R-12 °F·ft^2·h/BTU/in.) are 8.9×10^{17}, 1×10^{18}, and 1.2×10^{18} J (0.836, 0.951, and 1.101 quads), respectively [12].

Heat transport in porous materials is mainly contributed by conduction through solids and gases and radiation through voids [13–15]:

$$k_{eff} = k_{solid+gas+rad} \tag{1}$$

where k_{eff} is effective thermal conductivity. Heat transport through convection is usually negligible owing to the small pore size. At the condition of a small temperature gradient (e.g., when the temperature

* Corresponding author.
** Corresponding author.
E-mail addresses: shresthass@ornl.gov (S.S. Shrestha), tianli.feng@utah.edu (T. Feng).

https://doi.org/10.1016/j.ijthermalsci.2023.108164
Received 28 September 2022; Received in revised form 5 January 2023; Accepted 15 January 2023

difference ΔT is much smaller than the absolute average temperature T), the radiation contribution to thermal transport could be regarded as thermal conduction [13] with an equivalent thermal conductivity k_{rad}. Note that as pointed out by Tao et al., the solid and gas conduction as well as the radiation are usually coupled with each other [16,17] and should not be decomposed. To see more clearly their individual contributions, Eq. (1) is often written as the summation of effective solid, gas, and radiative thermal conductivities [15,17–27]:

$$k_{eff} = k_{solid} + k_{gas} + k_{rad} \tag{2}$$

Often, there is a trade-off between the conduction through solid and gas and radiation heat transfer. For example, increasing the porosity can reduce the solid thermal conductivity but will increase the gas and radiative thermal conductivities. Although air thermal conductivity is low, increasing porosity while porosity is high (>95%) will significantly increase radiative thermal conductivity, which will result in the increase of total thermal conductivity. Reducing the pore size can reduce the gas thermal conductivity, but it often decreases the porosity (for a constant wall thickness), thus increasing the solid thermal conductivity. Reducing the pressure reduces gas thermal conductivity but it requires sealing in barrier films, which induces higher costs. Therefore, lowering the overall thermal conductivity of thermal insulation materials economically is a challenge that requires an accurate understanding of the effect of the three components.

In the past few decades, significant efforts have been made to improve the theoretical understanding of thermal transport mechanisms in thermal insulation materials and push the thermal conductivity's lower limits [15,17–27]. Accordingly, many recent works have reviewed the progress of the theory and experiment in the design and development of new thermal insulation materials. For example, Shrestha et al. reviewed the models for solid conductivity [28]. Rezgar et al. reviewed the theoretical models for gas, solid, and radiative thermal conductivities for low-density polyethylene foams [15]. Walle reviewed the theoretical models, proposed a numerical framework to simulate the microscopic heat transfer at the pore scale, and studied the relationship between the pore structure and the effective thermal conductivity [18]. Hu et al. reviewed recent progress in developing porous materials for thermal insulation, focusing on strategies for creating gas voids [19]. Jelle reviewed the nano-based thermal insulation materials specifically for energy-efficient buildings [23]. Tang et al. reviewed thermal transport in particulate aerogels [24]. Liu et al. reviewed nano-cellular polymer foams focusing on polymer materials science and CO_2-based foaming strategies [25]. He et al. reviewed recent advances in thermal conductivity models of nanoscale silica aerogel insulation material [26]. However, most works focused singularly on specific types of materials, and models used for thermal conductivity are diverse. As a result, a model that works for aerogels might not work for foams, and a model developed for polyurethane form might not work for polystyrene. Due to the lack of a unified and validated model, it is difficult to develop new thermal insulation materials. In addition, the accommodation coefficient, an important factor that determines gas thermal conductivity, is seldom studied and unclear for most thermal insulation materials.

In this work, we attempt to unify the models for thermal transport in insulation materials that can cover a diverse range of types of insulation material. We have improved the literature models and calibrated and validated them through extensive experimental measurements of various thermal insulation samples with different porosities, pore sizes, gases, and pressures. With these, we decomposed the thermal conductivity into three components and propose the most efficient ways to further reduce the thermal conductivity of different porous materials. This work is aimed to provide a broader guideline to design the next generation of thermal insulation materials.

2. Literature review of theoretical models

2.1. Solid thermal conductivity models

Many models have been developed for estimating the effective thermal conductivity contributed by solids and gases together in porous materials [13,16,17,29–31]. Some decomposed models that account for the solid contribution only are provided in Table 1, including Russell [32], Maxwell-Eucken [33–35], Glicksman [36], and Bauer [37] models. These models have been frequently used in the literature [18–20,26,36,38–41]. A brief review of these models has been done by Shrestha et al. [28] and Rai et al. [42]. Since the Russell model in Eqs. (3) and (4) and the Maxwell-Eucken model in Eq. (5) do not consider the impact of struts that are usually presented in highly porous materials, Glicksman [36] modified the high-porosity approximation of the Russell model and derived the Glicksman model Eq. (6), where $0 \le f_s \le 1$ is the volume fraction of the solid in the struts. In addition, Bauer derived Eq. (7) based on spherical pores and introduced a geometry factor ξ to account for other shapes [37]. The best fit f_s and ξ values for the Glicksman and Bauer models are provided in Table 1 based on Ref. [42]. Note that these models only work for isotropic foams and not anisotropic foams, which have direction-dependent thermal conductivity.

The effective medium approximation (EMA) models assume that the solid material's intrinsic properties, including density, sound velocity, specific heat, and heat carriers' transport characteristic length, in the porous form are the same as those in the fully-dense bulk form. Although valid for polymer foams, this assumption does not hold for some materials such as aerogels. It has been reported that the sound velocity v decreases linearly with increasing porosity [43], and to account for the impact of sound velocity on thermal conductivity, Nilsson et al. proposed the following model [44]:

$$k_{solid}^{Nil}(\varphi, v) = k_s^0 \frac{\rho}{\rho_0} \frac{v}{v_0} \tag{8}$$

This model has been widely used in the literature [19,45–48]. In silica, Resorcinol-Formaldehyde (RF), Melamine–Formaldehyde (MF), and carbon aerogels [43],

Table 1
Solid thermal conductivity equations based on effective medium approximation. k_s^0 is the bulk thermal conductivity of a fully-dense solid, which depends on temperature. φ is porosity which denotes the ratio of the volume of voids to the total volume of the porous structure. The models only work for foams with isotropic thermal conductivity.

Effective medium approximation models for k_{solid}		Applicable structures	Eq. No.
Russell [32]	$k_{solid}^{EMA}(\varphi) = k_s^0 \frac{1-\varphi^{2/3}}{1-\varphi^{2/3}+\varphi}$	• Normal-packed hollow cubes • Truncated octahedrons (Voronoi structures)	(3)
Russell (high porosity limit) [32]	$k_{solid}^{EMA}(\varphi) = k_s^0 \frac{2}{3}(1-\varphi)$		(4)
Maxwell-Eucken [33–35]	$k_{solid}^{EMA}(\varphi) = k_s^0 \frac{1-\varphi}{1+\varphi/2}$		(5)
Glicksman [36]	$k_{solid}^{EMA}(\varphi) = k_s^0 \left(\frac{2}{3} - \frac{f_s}{3}\right)(1-\varphi)$	• $0 \le f_s \le 1$ for general foams • $f_s = 0.51$ for normal-packed hollow spheres • $f_s = 0.25$ for close-packed hollow spheres	(6)
Bauer [37]	$k_{solid}^{EMA}(\varphi) = k_s^0 (1-\varphi)^{1.5\xi}$	• $\xi = 0.783$ for Normal-packed hollow cubes • $\xi = 0.782$ for Voronoi foams • $\xi = 0.892$ for normal-packed hollow spheres • $\xi = 0.837$ for close-packed hollow spheres	(7)

$$\frac{v}{v_0} \approx \eta \frac{\rho}{\rho_0} = \eta(1-\varphi). \tag{9}$$

Here, v_0 and ρ_0 are the sound velocity and density of a fully-dense solid, ρ is the density of the porous material, η is a material-dependent constant, which is sensitive to the detailed material internal structures and manufacturing methods [43]. For example, heat-treated aerogels generally show higher sound velocities than untreated aerogels of the same density [43]. Based on these data, Gross and Fricke [43] fitted η values are around 0.78–1.25 for SiO_2 aerogels, 0.82 for carbon aerogels, 0.97 for MF aerogels, and 0.72–1.56 for RF aerogels. For some aerogels with low density ρ (e.g., <50 kg/m^3), the sound velocity may also depend on the gas pressure P [49]. Using the theoretical relations given by Gross et al. [49], we derived a simple equation that evaluates sound velocity as a function of sample density (porosity) and pressure:

$$\frac{v}{v_0} \approx \sqrt{\eta^2(1-\varphi)^2 - \frac{\varphi(P_{ambient}-P)}{\rho v_0^2}} \tag{10}$$

2.2. Models for gas thermal conductivity

The gas contribution to total thermal conductivity is usually written as

$$\kappa_{gas} = \varphi \kappa_g^0 \tag{11}$$

Here k_g^0 is the gas thermal conductivity in the diffusive regime. This model was developed by Glicksman [36] and has been widely used in the literature for thermal insulation materials [14,18,19,24,26,36,45,50–59]. When the pore size is comparable to or smaller than the gas mean free path, the Knudsen effect needs to be considered:

$$k_{gas}(P,T,\varphi,D) = \varphi \kappa_g^0(T) \frac{1}{1+2\beta\frac{\Lambda(P,T)}{D}} \tag{12}$$

Here, k_{gas} depends on pressure P, temperature T, porosity φ, and pore size D. $\Lambda(P,T) = \frac{k_B T}{\sqrt{2}\pi d^2 P}$ is the gas molecules' mean free path. d is the kinetic diameter of the gas molecules and k_B is the Boltzmann constant. A brief remark on the Knudsen effect is provided in the Supplementary Material. β is a parameter determined by the energy exchange rate between solid and gas molecules,

$$\beta = \beta_0 \cdot \frac{2-\alpha}{\alpha}, (0 \le \alpha \le 1) \tag{13}$$

where α is the energy accommodation coefficient between the gas molecules and the solid material [60]. The value of α is very important for thermal insulation materials, especially when the pore size is small (e.g., <1 μm) or pressure is low (e.g., <10 mbar). For example, in a 10 μ m pore at 10 mbar, k_{air} at 297 K is 7.5, 5.7, and 3.2 mW/m·K when α is 1.0, 0.8, and 0.5, respectively. More discussion on the significance of α is presented in Supplementary Material. The α value depends on the solid and gas materials, and the surface condition of the solid. It also depends on temperature, tending toward unity as the critical temperature of the gas is approached [61]. It is generally accepted that, except on surfaces with unusual preparation, common gases have α between 0.7 and 1 at room temperature [61]. Light gases, such as hydrogen and He, may have much lower α values [61]. The α values of most thermal insulation materials are unclear. Recently, Feng et al. [62] studied the energy exchange of He, Ar, N_2, and O_2 on the surface of polystyrene by all-atom molecular dynamics simulations and obtained α values in the range of 0.5–0.9. In Eq. (13), β_0 is the minimum value of β, when α takes its maximum value $\alpha = 1$. β_0 is usually determined by the thermal and kinetic properties of gas molecules [58,63,64]:

$$\beta_0 = \frac{1}{\mathrm{Pr}} \cdot \frac{2\gamma}{\gamma+1} \tag{14}$$

where Pr is the Prandtl Number, $\gamma = c_p/c_v$ is the specific heat ratio or adiabatic index, and μ is the absolute or dynamic viscosity. The value of β_0 is usually in the range of 1.5–2.0. Another less commonly used method to calculate β_0 is given by [65,66]

$$\beta_0 = \frac{5\pi}{32} \cdot \frac{9\gamma-5}{\gamma+1} \tag{15}$$

The β_0 values of some common gases are listed in the Supplementary Material.

2.3. Radiative thermal conductivity models

Radiation is generally considered as the most difficult mechanism to understand and accurately predict in porous materials, and it usually accounts for 20%–30% of the total heat transfer in high-porosity (φ >90%) materials [15,17–27]. For practical use, some simplified models are summarized in Table 2. Batty et al. [67] approximated the stacked cells as a series of parallel opaque planes that are separated by a distance that equals the cell size (D). That leads to Eq. (16), where ε_c is the cell wall emissivity, and σ_{SB} is the Stefan-Boltzmann constant. Batty et al. [67] also derived a radiative thermal conductivity model for when the surface emissivity is different from that of the cell walls. The Batty model significantly underpredicts the radiative component of heat transfer [18,36]. The largest limitation is that the model assumes each individual cell wall is opaque, which is not true since cell walls with <10 μ m thickness in most polymer insulation materials are highly transparent to the wavelength of the room-temperature radiation [36,68]. The other serious limitation is that the model assumes that the heat transfer between the two planes is pure radiation, which neglects its coupling with conduction and underpredicts k_{rad}. For instance, if there is no conduction, the radiative heat flux will be zero, and k_{rad} is zero, once any plane has zero emissivity. However, if conduction exists, it can bridge the heat transfer through these zero-emissivity planes and result in non-zero radiative heat flux (and non-zero k_{rad}).

Williams and Aldao [69] recognized that the cell walls in thermal insulation materials are highly transparent, and they improved the Batty model to Eq. (17), where L is the total thickness of the porous material along the temperature gradient direction, d_w is the cell wall thickness, r is the effective fraction of incident energy reflected by each wall, a is the absorption coefficient of the solid material (average value over the range of wavelengths of the radiant energy), t is the effective fraction of radiant energy transmitted through each wall, T_N is the net fraction of radiant energy transmitted by each cell wall, and n_s is the refractive index of the solid material (when porosity is zero). The values of a and n_s are 1.51 and 6.61 × 10^{-2} μm^{-1} for polyolefin [75] and 1.59 and 7.53 × 10^{-3} μm^{-1} for polystyrene [69], respectively. This model is suitable for cellular foams with cell walls dominating over struts and has worked well for polyethylene foams [15,75–79], Al foams [76], polymethyl methacrylate (PMMA), and poly(methyl methacrylate)-poly(butyl acrylate)-poly(methyl methacrylate) (MAM) foams [14].

Compared with the Batty and Williams–Aldao models, a more rigorous theory of the radiation in porous materials starts from Beer's law, with which the transmissivity (Tr) of a material decays exponentially with thickness [36]: $Tr \propto \exp(-K \cdot L) = \exp\left(-\frac{L}{\mathrm{MFP}_{\mathrm{photon}}}\right)$, where K, with the units of inverse length, is the extinction coefficient, L is the thickness of the sample, and $\mathrm{MFP}_{\mathrm{photon}} = 1/K$ is the mean free path (MFP) of photons. Thermal insulation materials are usually optically thick since the typical photon MFP (≤1 mm) is much smaller than the sample thickness [36]. The most accurate way to determine K is through the integration of the spectral extinction coefficient e_λ by Eq. (18) [20,70,71,80,81]. Here e_λ is the spectral extinction coefficient of the porous material, λ is the wavelength of radiation, $E_{b\lambda}$ is the spectral blackbody radiation intensity at a given temperature, and E_b is the integrated blackbody intensity at a given temperature. e_λ can be determined by theoretical calculations or experimental measurements. For cellular

Table 2
Models for radiative thermal conductivity in thermal insulation materials.

Models		Equations	Parameters	Eq. No.
Batty [67]		$k_{rad} = \frac{4D}{\left(\frac{2}{\varepsilon_c}-1\right)}\sigma_{SB}T^3$	–	(16)
Williams–Aldao [69]		$k_{rad} = \frac{4\sigma_{SB}T^3L}{1+\frac{L}{D}\left(\frac{1}{T_N}-1\right)}$	$T_N = \frac{1-r}{1-rt}\left[\frac{(1-r)t}{1+rt}+\frac{1-t}{2}\right]$ $r = \frac{(n_s-1)^2}{(n_s+1)^2}$ $t = \exp(-ad_w)$	(17)
Rosseland	Spectral [70,71]	$k_{rad} = \frac{16n^2}{3K}\sigma_{SB}T^3$ $K \equiv \frac{1}{MFP_{photon}}$	$K = \left[\int_0^\infty \frac{1}{e_\lambda}\frac{\partial E_{b\lambda}}{\partial E_b}d\lambda\right]^{-1}$	(18)
	Kuhn [70]		$K = (f_s e_s + (1-f_s)e_w)\rho$	(19)
	Hsu–Howell [72]		$K = \frac{3}{D}(1-\varphi)$	(20)
	Hendricks–Howell [73]		$K = \frac{C_m}{D}(1-\varphi)$	(21)
	Glicksman– Torpey [39]		$K = \frac{C_m}{D}\sqrt{1-\varphi}$	(22)
	Glicksman [36]		$K = \frac{4.1}{D}\sqrt{f_s\frac{\rho}{\rho_0}}+(1-f_s)\frac{\rho}{\rho_0}K_w$	(23)
	Tao [74]		$K = 42.038\rho + 121.55$	(24)

foams such as polymer and metallic foams, the total extinction coefficient is contributed by cell walls and struts [70,71] shown in Eq. (19). e_s (m^2/kg) is the specific extinction coefficients of struts, which depends on the strut diameter (d_s) and can be calculated via the Mie theory. f_s is the strut fraction in a solid. e_w (m^2/kg) is the specific extinction coefficient of the cell walls, which depends on the cell wall thickness (d_w) and can be calculated via Snell's law. Kuhn et al. [70] and Placido et al. [71] calculated e_s and e_w for polystyrene. Although Eq. (19) can provide accurate results, the spectral extinction coefficient calculation is complicated and, hence, some simplified models have been developed to determine K in the literature.

Hsu and Howell developed Eq. (20) for K that depends only on the average pore size, D, and porosity, φ, based on the experimental data of porous zirconia (ZrO_2) [72]. The Hsu-Howell model works for porous materials made of dispersed pores in a solid matrix with a pore size larger than 0.6 mm [72,82,83]. It has been widely used in cellular (reticulated) ceramic foams for solar energy collection and fuel combustion [82–87], and the materials are not limited to ZrO_2 but also yttria-stabilized zirconia/alumina composites, mullite, cordierite [86], alumina, silicon carbide (SiC), and FeCrAl [87].

Hendricks and Howell later revised the Hsu-Howell model by adjusting the coefficient 3 to be a material-dependent constant C_m, as shown in Eq. (21). They fitted the value of C_m to be 4.4 for reticulated porous partially stabilized zirconia and 4.8 for oxide-bonded SiC. Furthermore, it is found that 4.8 is suitable for solar dish systems based on SiC [88], and 4.4 is suitable for porous ceria (CeO_2) [89]. Glicksman and Torpey [39] assumed that the cell walls are transparent, and the extinction coefficient is proportional to the total surface area of the strut per unit volume, which is proportional to $\frac{\sqrt{1-\varphi}}{D}$, assuming that the cells are pentagonal dodecahedrons and the struts are inscribed within equilateral triangles. Finally, they give Eq. (22). C_m depends on pore and strut geometries. Glicksman and Torpey [39] proposed the value of C_m to be 3.68. Later, the geometric coefficient C_m was revised to 2.64 by Cunsolo et al. [90], 2.71 by Li et al. [91], and 2.656 by Loretz et al. [92]. Cunsolo et al. [90] also proposed a model considering that the diameter of a strut is not uniform $K = \frac{2.62[1-0.22(1-l_t)^2][1+0.22(1-l_k)^2]}{D}\sqrt{1-\varphi}$. The parameter l_t is defined as the ratio of the minimum to the maximum diameter of struts, $0 \le l_t \le 1$. l_k is defined as the ratio of the curvature radius of the circle circumscribing of the triangle to the local signed curvature radius of the sides, $-0.3 \le l_t \le 1$. This model was found to be more accurate than the Glicksman–Torpey model [90,91].

Glicksman [36] included the contribution from cell walls and proposed Eq. (23). The coefficient 4.1 is a constant related to the cell geometry and is determined by assuming the pores are dodecahedra. K_W is the extinction coefficient of the solid material. The K_W values for polyolefin [15,36,77,93], polystyrene [15,36,94], and polyurethane (PUR) [36,95,96] are 140 ± 20 cm^{-1}, 80 cm^{-1}, and 600 cm^{-1}, respectively. Glicksman's model has been extensively used for polymer foams [15,36,77,93–96]. Tao et al. fitted K for PUR in Eq. (24), which is only dependent on the sample density. Tao's model has been used for PUR [97,98], foam insulation [99], metal foam [100], and syntactic composite foams made of hollow carbon microspheres as the filler and APO-bismaleimide resin as the binder [101].

3. Improvement of theoretical models

The solid and gas thermal conductivity models in Section 2 have several drawbacks. The EMA model can account for the impact of the loss of mass on solid thermal conductivity but cannot include the effect of sound velocity softening. The Nilsson model can account for the effect of sound velocity softening but oversimplified the effect of loss of mass by using a factor $\frac{\rho}{\rho_0} = (1-\varphi)$. Therefore, an accurate model that can correctly account for both effects should be

$$k_{solid}^{new}(\varphi, v) = k_{solid}^{EMA}(\varphi)\frac{v}{v_0} \tag{25}$$

where $k_{solid}^{EMA}(\varphi)$ is obtained by the EMA models listed in Eqs. (3)-(7). This new model should not only work for insulation materials but also for general porous materials with low porosity.

The gas thermal conductivity model (Eq. (11)) has been widely used in the literature for thermal insulation materials [14,18,19,24,26,36,45,50–59]. However, it was derived and simplified from the following EMA model

$$\kappa_{gas}^{new} \approx \frac{\varphi^{\frac{2}{3}}}{1-\varphi^{\frac{2}{3}}+\varphi}k_g^0 \approx \frac{\varphi+\frac{1}{2}}{1+\frac{\varphi}{2}}\kappa_g^0 \tag{26}$$

See the Supplementary Material for detailed derivation. Compared to Eq. (26), Eq. (11) is over-simplified, and the difference is prominent at lower porosities. Since gas thermal conductivity usually dominates over solid conduction and radiation, this difference will be important for the overall thermal performance.

Since pore sizes in most materials are not uniform, it has been widely adopted to use a pore size distribution [56,102] to account for the Knudsen effect [63] of gas conduction. Here, we simplify the pore size distribution to two pore sizes. Combined with Eq. (26), the one-pore size and two-pore size models are

$$\kappa_{gas}^{new}(P,T,\varphi,D)=\frac{\varphi+\frac{1}{2}}{1+\frac{\varphi}{2}}\kappa_g^0(T)\frac{1}{1+2\beta\frac{\Lambda(P,T)}{D}} \tag{27}$$

and

$$\kappa_{gas}^{new}(P,T,\varphi,D_1,D_2,f)=\frac{\varphi+\frac{1}{2}}{1+\frac{\varphi}{2}}\kappa_g^0(T)\cdot\left(\frac{f}{1+2\beta\frac{\Lambda(P,T)}{D_1}}+\frac{1-f}{1+2\beta\frac{\Lambda(P,T)}{D_2}}\right) \tag{28}$$

respectively. Here, the pore with size D_1 has a volume fraction f and D_2 has a volume fraction $1-f$. $f = V_1/(V_1 + V_2)$, where V_1 and V_2 are the total volumes of the pores with size D_1 and D_2, respectively. The one and two-pore size models will be examined on various materials.

4. Experimental methodology

The accuracy of the models discussed in section 2 is examined through extensive experimental measurements on various existing commercially available thermal insulation materials. Moreover, we extracted the individual solid, gas, and radiation contributions to the overall thermal conductivity, which facilitates the design of the next generation of improved thermal insulation materials. We choose expanded polystyrene (EPS), high-density EPS (HD-EPS), PUR foams, PUR-based aerogels, fumed silica used in vacuum insulation panels (VIPs), and Standard Reference Material (SRM) 1449 fumed silica board as the diverse systems for a comprehensive study. The sample properties, including materials compositions, densities, porosities, and average pore sizes, are listed in Table 3. Most of these materials have high porosity, varying between 88.2% and 98.6%. The microstructures were characterized by scanning electron microscopy (SEM), as shown in Fig. 1. The pore size ranges from 0.16 to 700 μ m. The average pore sizes for the first three samples are estimated from the SEM images, and those for the last three samples are discussed in Sec. 3.3.

The thermal conductivity was measured following the standard Test Method [103], as shown in Fig. 2. The test setup consists of Fox 200 Heat Flow Meter Apparatus enclosed in a sealed chamber, a roughing pump, a turbo pump, and three pressure gauges. All samples are 20 × 20 cm^2, with thicknesses varying from 13 to 30 mm, sandwiched between two black plates with temperatures of 55 F and 95 F, respectively. The heat fluxes q of the two plates are monitored by the system, and the thermal conductivity is extracted from the Fourier law: $\kappa_{eff} = \frac{q}{A\Delta T}L$, where A is the surface area, ΔT is the plates' temperature difference, and L is the sample thickness. Since the materials are open-cell materials, we evacuated the samples and measured the pressure-dependent thermal conductivity. When the pressure is below 20 mbar, the Agilent Varian CDG 500, a deep vacuum gauge, is used to monitor the pressure, which has an uncertainty of 0.2%. For higher pressures, the pressure gauge MKS Baratron Pressure Transducer Model 750B with an uncertainty of 1% and Omega DPG104S with an uncertainty of 0.25% are used. The measurement error also includes the general 3% uncertainty of the Fox 200 Heat Flow Meter Apparatus.

Table 3
Properties of the insulation materials studied in this work.

Samples	Materials	Density ρ (kg/m^3)	Porosity φ
EPS	Polystyrene	13.81	98.62%
HD-EPS	Polystyrene	30.60	96.94%
PUR	Polyurethane	29.15	97.52%
PUR aerogel	Polyurethane	123.50	89.50%
Fumed Silica (VIP core)	Silica (TiO_2 and carbon as opacifiers)	196.23	91.08%
SRM 1449, Fumed-Silica Board	60% SiO_2 + 35% $FeTiO_3$ + 5% ceramic fiber	330.94	88.17%

5. Validation of improved theoretical models

5.1. Validation of solid thermal conductivity model

The improved solid conduction model (Eq. (25)) is examined against the EMA models (Eqs. (3-7)) and Nilsson's scaling model (Eq. (8)). The materials selected for the comparison need to satisfy two criteria for better and accurate validation. First, the materials should have velocity softening relative to the fully dense solid counterpart, in order to differentiate the improved models from EMA models. This excludes the cellular polymer foams. Second, the materials should not have too high porosity (>95%), otherwise, the measured evacuated thermal conductivity contains radiative thermal conduction, which may induce unnecessary uncertainty for solid conduction validation. We collected silica VIP core, SRM 1449 fumed silica board, and calcium silicate insulation, with detailed information listed in Table 4. The porosity ranges from 78% to 91%. The thermal conductivity measured at <0.01 mbar is shown in Table 4, which can be viewed as k_{solid} since radiation is negligible. The theoretical density of the fully-dense solid is calculated based on the composition, and velocity scaling is read from the literature data based on the relative density. The fully dense solid thermal conductivities, k_s^0, of silica and calcium silicate are obtained from the literature [104]. Two RF aerogels [105] from the literature are also included for examination. k_s^0 and ρ_0 are obtained from Bakelite [65]. Fig. 3 shows the comparison of the models. EMA models, which do not account for sound velocity softening, overestimate the thermal conductivity significantly. The Nilsson scaling overestimates the thermal conductivity by 30%–50%.

5.2. Validation of gas thermal conductivity model

The modified gas thermal conductivity model is examined. First, we compare the factor in front of k_g^0 in the modified model (Eq. (26)) and the original model (Eq. (11)). As shown in Fig. 4 (a), the original model, which simply uses φ as the factor, largely underpredicts the gas thermal conductivity. This underprediction is more prominent at lower porosity. For most thermal insulation materials with porosity >95%, this underprediction is too small to visualize. But for general porous materials, this effect might not be negligible. To validate the improved model, the model k_{gas} is compared to the experimental k_{gas}, which is obtained by subtracting k_{eff} of evacuated samples from the k_{eff} of ambient-pressure samples. For a better and more accurate validation, we only include the samples with large pore sizes, in order to avoid the unnecessary uncertainty brought by the Knudsen effect in small pores and the unclear thermal accommodation coefficient. We took the literature porous materials (porous plastics, beef, apple, and pear with φ of 0.85, 0.76, 0.86, and 0.87, respectively [106]) as well as our own porous foams (EPS, HDEPS, and PUR foam) as examples to demonstrate the difference. As shown in Fig. 4 (b), the improved model gives more accurate results in general. This improvement could be important when the design of ultra-low thermal conductivity materials heads toward the low porosity end and when 1 mW/mK makes a difference.

5.3. One-pore vs. two-pore gas thermal conductivity models

To examine whether a pore size distribution is needed to reproduce the pressure-dependent thermal conductivity [51,56,57,89,102,107], we attempted to use the one-pore and two-pore models to fit the experimental data. When fixing all the other conditions except pressure, the effective thermal conductivity can be written as

$$k_{eff}(P)=k_g^0\frac{\varphi+\frac{1}{2}}{1+\frac{\varphi}{2}}\frac{1}{1+\frac{A}{P}}+C \tag{29}$$

and

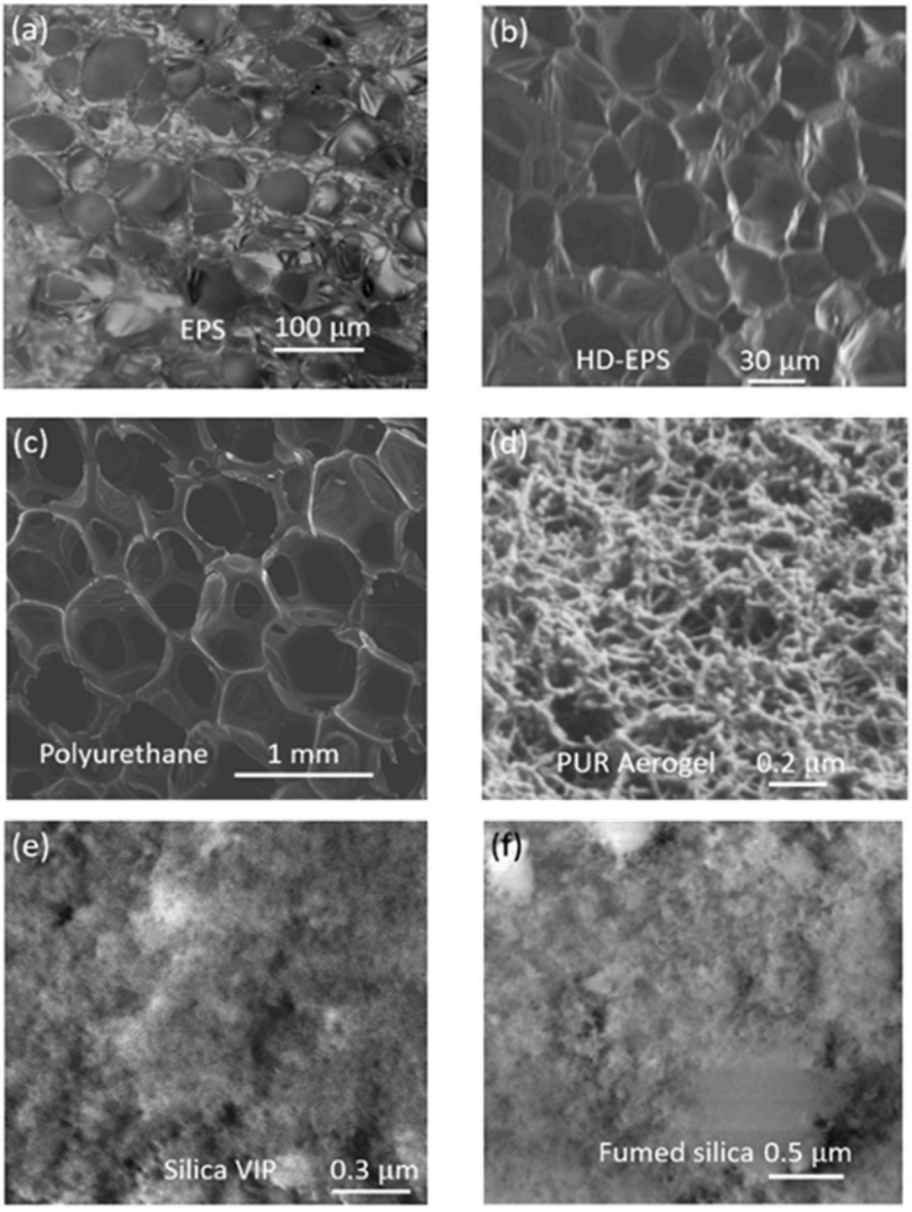

Fig. 1. SEM images of the thermal insulation materials studied in this work. (a–c) EPS, HD-EPS, and PUR foams are cellular foams, and (d–f) PUR aerogel, silica VIP, and SRM 1449 fumed silica are granular forms.

Fig. 2. Thermal conductivity measurement apparatus. (Left) FOX 200 Heat Flow Meter Apparatus enclosed in a sealed chamber. (Right) Vacuum pump.

$$k_{eff}(P) = k_g^0 \frac{\varphi + \frac{1}{2}}{1 + \frac{\varphi}{2}} \left(\frac{f}{1 + \frac{A_1}{P}} + \frac{1 - f}{1 + \frac{A_2}{P}} \right) + C \tag{30}$$

for the one-pore and two-pore models, respectively. Here, $A = 2\beta \frac{k_B T}{\sqrt{2}\pi d^2 D}$, $A_1 = 2\beta \frac{k_B T}{\sqrt{2}\pi d^2 D_1}$, $A_2 = 2\beta \frac{k_B T}{\sqrt{2}\pi d^2 D_2}$, $C = k_{solid} + k_{rad}$, and f are pressure-independent constants and thus fitting parameters. As shown in Fig. 5, both models fit well the experimental data, with the two-pore model performing better, indicating that at most two pore sizes are needed to reproduce the pressure-dependent thermal conductivity while a complex pore size distribution is unnecessary. To further verify this, we also fit the experimental data in the literature. As shown in Fig. 6 (porous plastics) and Fig. 7 (porous beef), the two-pore model fits well all the data (with an average $R^2 = 0.9976$) [106]. The fitting is also good for porous apple, pear [106], silica [107,108], RF [105] and xonotlite aerogels [109] (see the Supporting Information).

Table 4
Modeled and measured solid thermal conductivity of porous materials. RF0.6 and RF7 aerogels data are taken from Ref. [105], while the others are measured in this work. * k_{solid} was measured in a vacuum and consists of both solid conduction and radiative conduction. As discussed in the main text, radiative conduction is negligible in these samples due to either high density or high extinction coefficients.

Materials/ Properties	Silica VIP core (this work)	SRM 1449, Fumed-Silica Board (this work)	Calcium silicate (this work)	RF 0.6	RF 7
ρ (g/cm^3)	0.196	0.331	0.62	0.33	0.32
ρ_0 (g/cm^3)	2.2	2.8	2.9	1.35	1.35
ρ/ρ_0	0.08918	0.11832	0.21379	0.24444	0.23704
v/v_0	0.059 ± 0.011	0.091 ± 0.025	0.21 ± 0.02	0.26 ± 0.03	0.25 ± 0.03
φ	0.9108	0.8817	0.7862	0.7556	0.7630
k_s^0 (W/mK)	1.4	1.4	1.1	0.23	0.23
EMA, Eq. (3-7) (W/mK)	85.79	114.97	168.81	40.81	39.46
sound velo scaling, Eq. (8) (mW/mK)	7.37 ± 1.40	15.07 ± 4.22	48.77 ± 4.88	14.56 ± 1.46	13.63 ± 1.36
EMA + sound scaling, Eq. (25) (mW/mK)	5.06 ± 0.96	10.46 ± 2.93	35.01 ± 3.50	10.57 ± 1.06	9.87 ± 0.99
Experimental k_{solid}* (mW/mK)	4.0	7.52	34.6	10.0	11.0

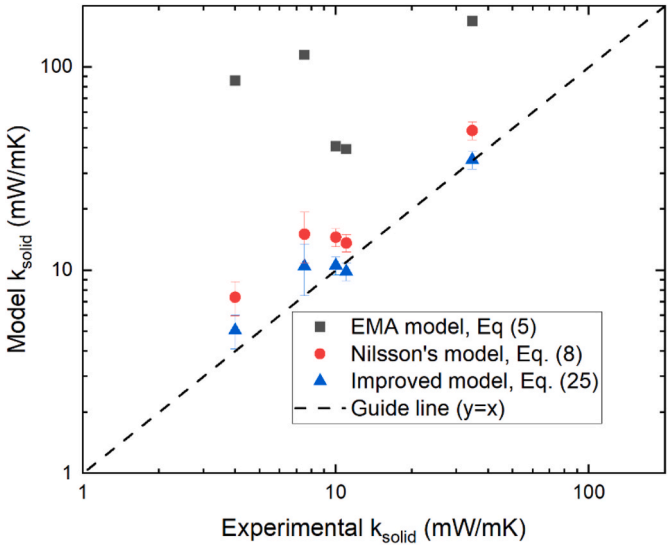

Fig. 3. Comparison of three different models for solid conduction in porous materials. The detailed materials' properties are listed in Table 4.

6. Thermal conductivity decomposition for EPS, HD-EPS, PUR foam, PUR aerogel, and silica-VIP cores

6.1. EPS and HD-EPS

After k_{gas} is obtained, we calculate k_{solid} and k_{rad} to validate $k_{gas}+k_{solid}+k_{rad}$ against the experimental k_{eff} data. For EPS, k_{solid} can be calculated by EMA models with $f_s = 0$ in Table 1. Taking the bulk fully dense polystyrene thermal conductivity $k_s^0 = 0.16$ W/m·K [110], we estimate k_{solid} of EPS as 1.44 mW/m·K, as shown in Fig. 8.

For evaluating the radiation component, the most accurate method is through the Rosseland model with the extinction coefficient calculated by the spectral integration using Eq. (18). Kuhn et al. [70] did this calculation for polystyrene and obtained the specific extinction coefficients of cell walls (e_w) and struts (e_s) in polystyrene as functions of cell wall thickness (d_w) and strut diameter (d_s), respectively. Therefore, we can use Kuhn et al.'s results to evaluate the k_{rad} in our EPS sample using Eq. (19).

To do that, we need to determine the d_w, d_s, and f_s (volume fraction of struts) of our EPS. Since EPS usually does not have struts [71] ($f_s = 0$, $d_s = 0$), we only need the d_w value. However, directly measuring d_w is difficult. For this, Placido et al. [71] proposed a formula to calculate d_w and f_s using d_s and D, based on the geometry model proposed by Kuhn et al., in which cells, walls, and struts are modeled respectively like regular pentagonal dodecahedrons, thin slabs (platelets), and cylinders [70]. d_w and f_s are given by

$$d_w = \frac{0.348(1-\varphi)D^3 - 2.8d_s^2D + 3.93d_s^3}{1.3143D^2 - 7.367d_sD + 10.323d_s^2} \tag{31}$$

$$f_s = \left[1 + \frac{(1.3143D^2 - 7.367d_sD + 10.323d_s^2)d_w}{2.8d_s^2D - 3.93d_s^3}\right]^{-1} \tag{32}$$

When struts are negligible ($f_s = 0$), the cell wall thickness solely depends on porosity and pore size. Equation (31) is reduced to $d_w = C_w(1-\varphi)D$, where C_w is a constant depending on the geometry of the pores. C_w = 0.265, 0.461, 0.323, and 0.264 for regular pentagonal dodecahedrons, cubes, normally stacked hollow spheres, and tightly stacked hollow spheres, respectively (See Supplementary Material for detailed derivation). For cubes, D is the equivalent diameter of a spherical pore with the same volume as the cube. For stacked hollow spheres, D is not the diameter of each sphere but rather the average diameter of all the voids, including the hollow spheres and the void spaces encompassed between the adjacent spheres. The four C_w values result in d_w of 0.174, 0.318, 0.223, and 0.173 μ m, respectively. The calculated $k_{gas}+k_{solid}+k_{rad}$ agrees well with the experimental k_{eff} data in general with an average error <7%, as shown in Fig. 8. In comparison, the other k_{rad} models do not replicate well the experimental data in this study, except for Tao's model, which agrees reasonably well with the experiment considering a certain amount of uncertainty.

Similarly, for HD-EPS, k_{solid} is also calculated with EMA models with $f_s = 0$, which give $k_{solid} \approx 3.15$ mW/m·K, as shown in Fig. 9. Here we use $C_w = 0.265$ to evaluate the wall thickness since the cells of HD-EPS can be well represented by pentagonal dodecahedrons rather than cubes or spheres. The obtained d_w is 0.406 μ m. Knowing the d_w value, we calculated k_{rad} by using Kuhn et al.'s extinction coefficient. The calculated $k_{gas}+k_{solid}+k_{rad}$ agrees well with experimental data (with an error <2%), as shown in Fig. 9. In addition to that from Kuhn's model, the extinction coefficient from Tao's model also agrees well with the experimental data, which indicates that Tao's model fitted from PUR data in the literature may also work for other polymers (e.g., polystyrene).

6.2. PUR foam and PUR aerogel

The predictions for PUR are more complicated to estimate than for polystyrene because the former represents a category of materials rather than a specific one, and there is no exact chemical formula for this compound. Therefore, solid PUR has a broad range of thermal conductivity values reported in the literature, from 0.21 to 0.26 W/m·K [36,70,95,96,111], a broad range of densities from 1.145 to 1.225 g/cm^3 [95,111–114], and a radiative property that is not predictable owing to the lack of an exact chemical formula [70,71].

For the PUR foam, k_{solid} is evaluated with EMA models with $f_s = 0$. Taking $k_s^0 = 0.235 \pm 0.025$ W/m·K and $\rho_0 = 1.177 \pm 0.030$ g/cm^3, k_{solid} is estimated as 3.91 ± 0.68 mW/m·K. After examining all the k_{rad} models, we found that the Rosseland equation (with the extinction coefficients calculated by the Tao model, the Glicksman model, and the

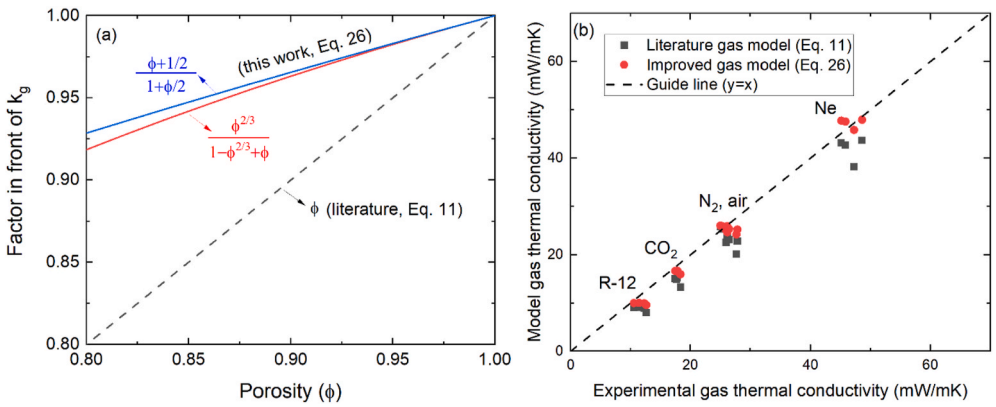

Fig. 4. Comparison between literature and improved gas thermal conductivity model. Experimental data in (b) include both literature data [106] and this work.

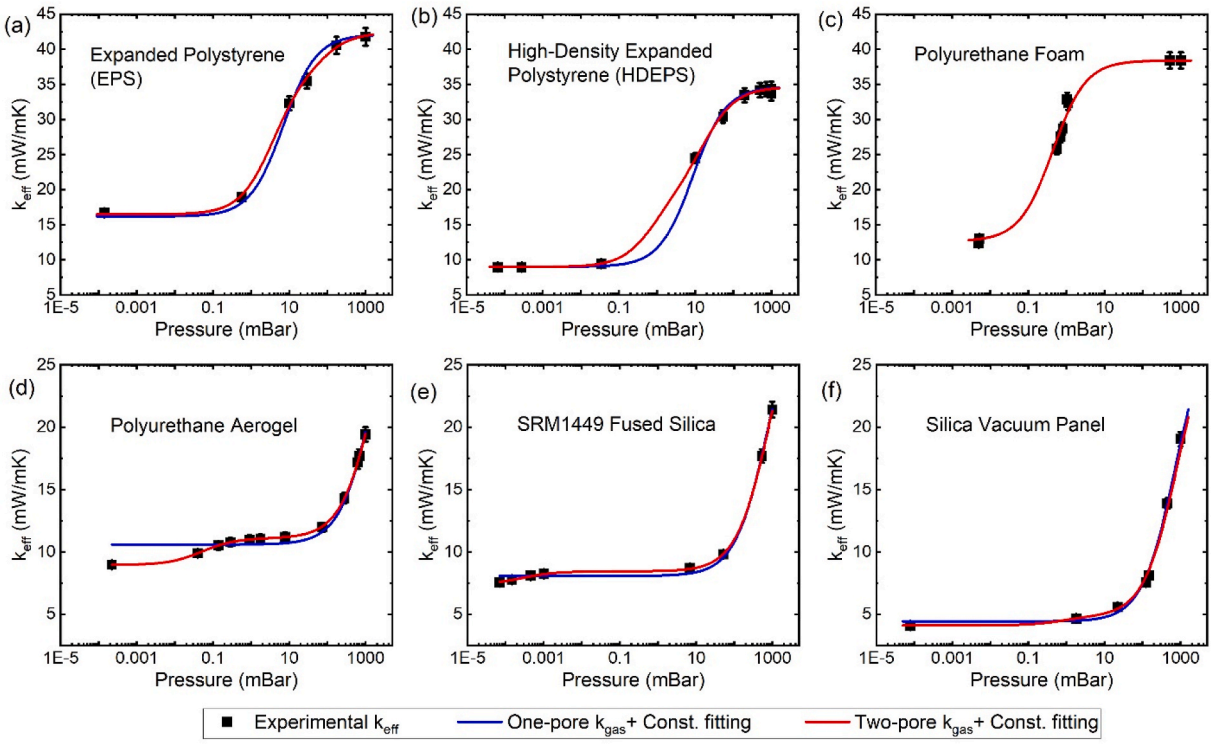

Fig. 5. Effective thermal conductivity as a function of pressure. All experiments are done at 297 K with pores filled with air. The blue and red curves represent the one-pore and two-pore model fittings, respectively. The error bars for experimental data are from the measurement uncertainty, 3%, given by the apparatuses. In (c), blue and red curves overlap.

Glicksman-Torpey model) agrees well with the experimental data, whereas the others, such as the Batty model, give a large discrepancy, as shown in Fig. 10.

For the PUR aerogel, since the structure is network-like rather than cellular, we use the Glicksman model (i.e., Eq. (23)) with a high strut fraction (>90%) to evaluate k_{solid}, which is approximately 9.05 ± 1.58 mW/m·K, as shown in Fig. 11. If the radiative thermal conductivity is evaluated by Tao's model, which gives k_{rad} = 1.65 mW/m·K, the total $k_{gas} + k_{solid} + k_{rad}$ is higher than the experimental k_{eff}. Since Tao's model [74] was fitted for PUR foam with unrealistically larger pore sizes (D~10^2 μ m) than our PUR aerogel (D~10^{-1} μ m), we suspect that it strongly overestimates k_{rad} of PUR aerogel since k_{rad} is generally proportional to pore size. Therefore, we suspect that the k_{rad} in our PUR aerogel is much lower than that predicted by Tao's model. Indeed, after examining the other k_{rad} models discussed in Sec. 2.4, we find that most of them give negligible k_{rad}, i.e., $k_{rad} \approx 0$. With this, the total calculated $k_{gas} + k_{solid} + k_{rad}$ values agree very well with the experimental k_{eff}, as shown in Fig. 11.

6.3. Silica-based VIP-core materials

For the fumed silica VIP core and SRM 1449, the radiative thermal conductivity is negligible since the pore size is small (<1 μ m), porosity is not high (88%–91%), and opacifiers are added to the materials. Therefore, $k_{solid} = k_{eff}$ ($P \approx 0$), as shown in Figs. 12 and 13. The predictions have error bars because the sound velocity of porous silica with a given density has a broad range of uncertainty. That is, for SiO_2 samples with the same density, the sound velocity can vary by a considerable amount.

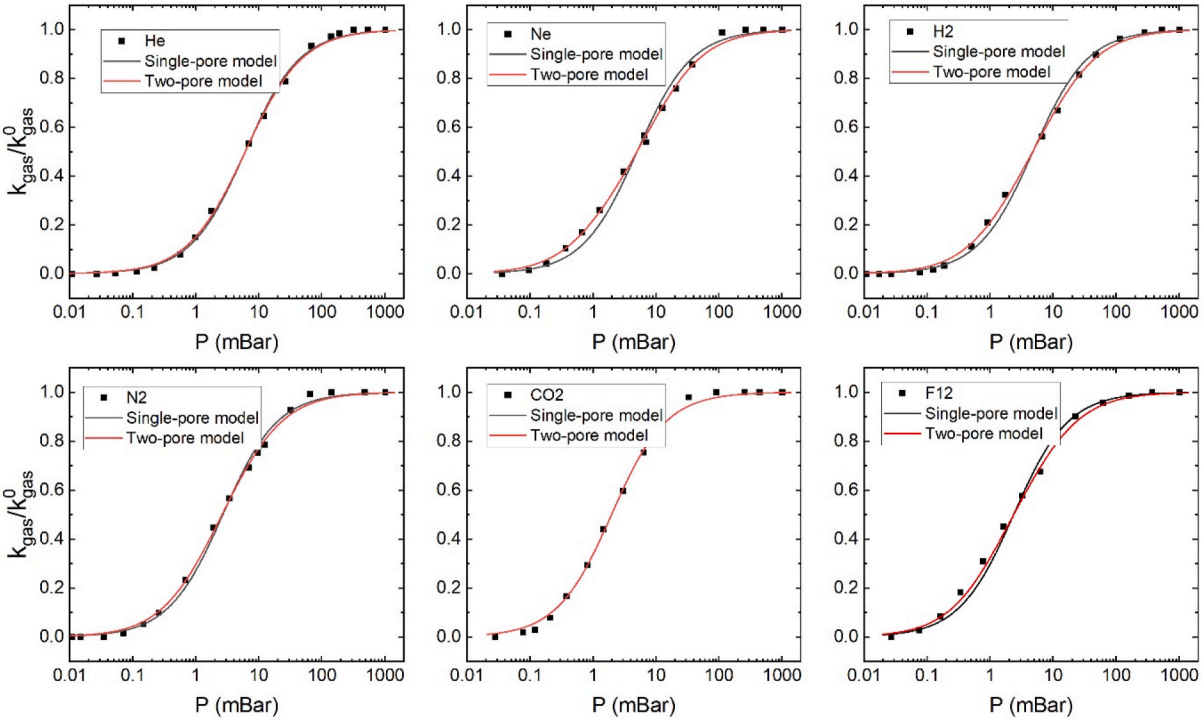

Fig. 6. One-pore and two-pore size fitting of gas thermal conductivity for the plastics filled with various gases studied by Harper and Sahrigi [106].

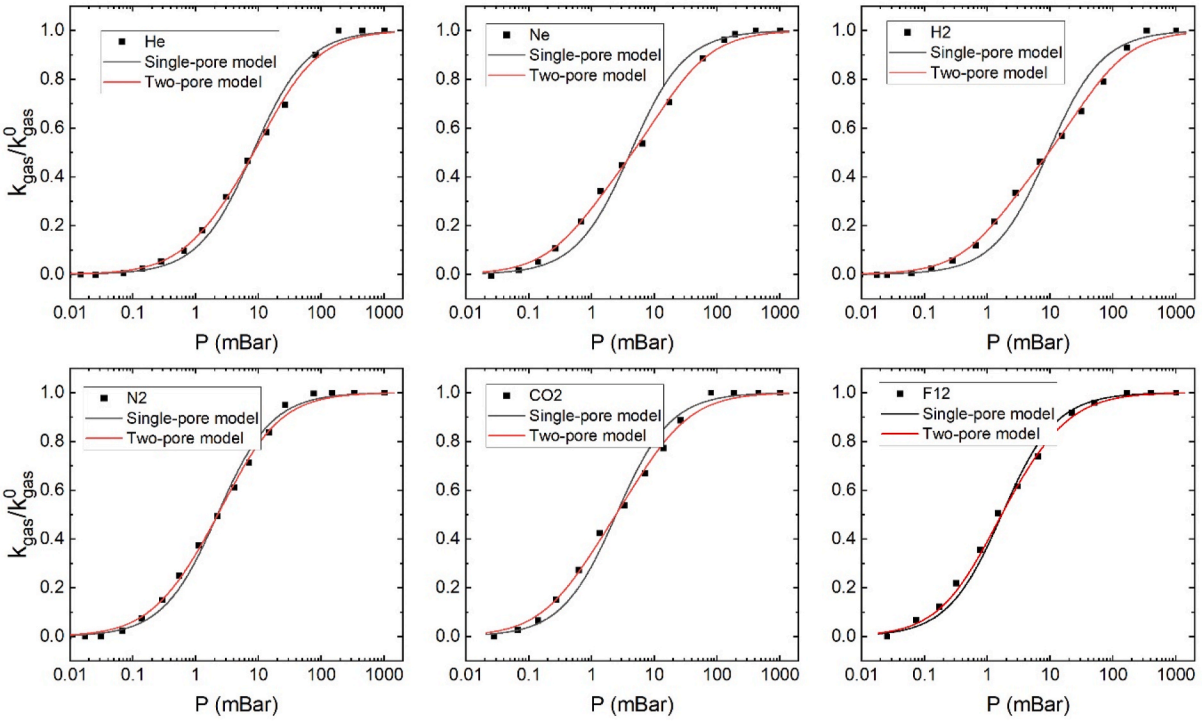

Fig. 7. One-pore and two-pore size fitting of gas thermal conductivity for the porous beef filled with various gases studied by Harper and Sahrigi [106].

6.4. *Relative contribution of k_{gas}, k_{solid}, and k_{rad} to k_{eff}*

To determine the dominant heat transfer mechanisms and find optimal strategies to reduce effective thermal conductivity, the individual k_{gas}, k_{solid}, and k_{rad} are summarized in Fig. 14. For polymer foams (EPS, HD-EPS, and PUR in this work), k_{gas} and k_{rad} dominate the thermal conductivity whereas k_{solid} is very small, indicating that the most efficient way to reduce the effective thermal conductivity of cellular polymer foams is to reduce the pore size, which can simultaneously reduce k_{gas} and k_{rad}. Since the pore size in these foams is currently around 10–10^3 μ m, there is a large space to reduce the pore size. Reducing pore size may sacrifice some porosity and increase k_{solid}, but this will not offset the decrease in k_{gas} and k_{rad} since k_s^0 is low. Therefore, identifying strategies to manufacture nano-cellular polymer foams is a

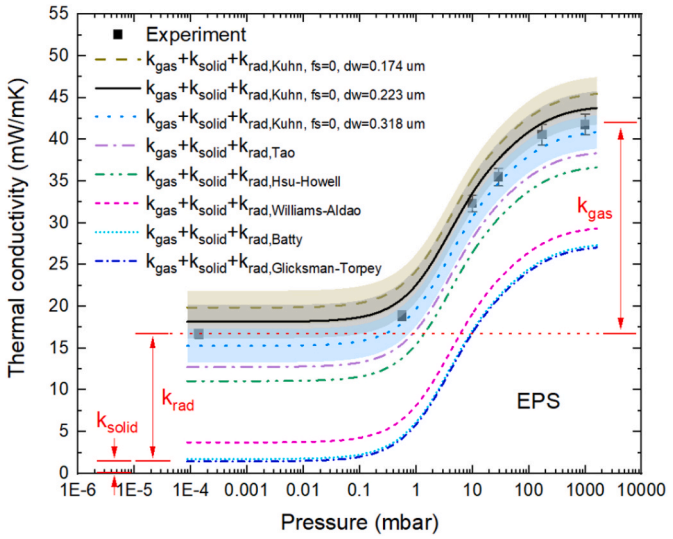

Fig. 8. The model prediction of $k_{gas} + k_{solid} + k_{rad}$ compared with experimental data (k_{eff}) for EPS filled with air at 297 K as a function of pressure. Curves are theoretical predictions with different radiation models. The shaded area indicates the prediction uncertainty with the Kuhn model. This sample has a porosity of 98.62% and a density of 0.0138 g/cm^3.

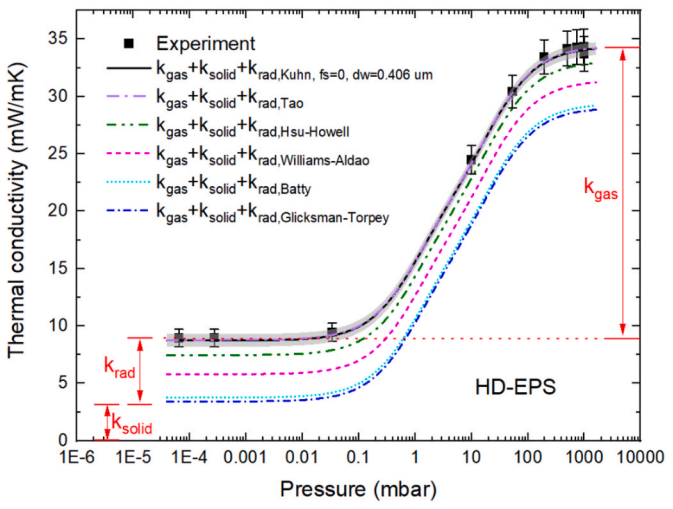

Fig. 9. The model prediction of $k_{gas} + k_{solid} + k_{rad}$ as compared with experimental data k_{eff} for HD-EPS filled with air at 297 K as a function of pressure. Curves are theoretical predictions with different radiation models. The shaded area indicates the prediction uncertainty. This sample has a porosity of 96.94%, and a density of 0.0306 g/cm^3.

promising direction for the next generation of thermal insulation materials.

For aerogels (PUR aerogel, silica VIP, and fumed silica), the dominant thermal conductivity components are k_{gas} and k_{solid} whereas k_{rad} is negligible owing to the small pore size and the addition of opacifiers. Although the pore size is already $\sim 10^{-1}$ μ m, if new manufacturing methods can further reduce it to ~10 nm while maintaining the porosity, significantly reduced k_{eff} can be achieved. For inorganic materials, k_s^0 is generally high; hence, it might not be ideal to decrease porosity, which can significantly increase k_{solid}. Therefore, more opportunities should be sought in engineering polymers that have small k_s^0. For example, in the case of PUR aerogel, which has $k_{gas} = 10.5$ mW/m·K and $k_{solid} = 9.0$ mW/m·K, the best strategy is to further reduce the pore size while maintaining porosity. Another strategy is to replace PUR with

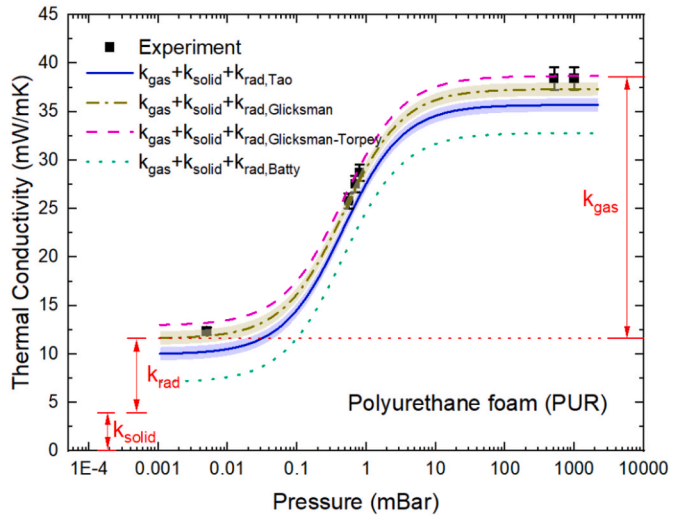

Fig. 10. The model prediction of $k_{gas} + k_{solid} + k_{rad}$ as compared with experimental data k_{eff} for PUR foam filled with air at 297 K as a function of pressure. Curves are theoretical predictions with different radiation models. The shaded area indicates the prediction uncertainty. This sample has a porosity of 97.52%, and a density of 0.0292 g/cm^3.

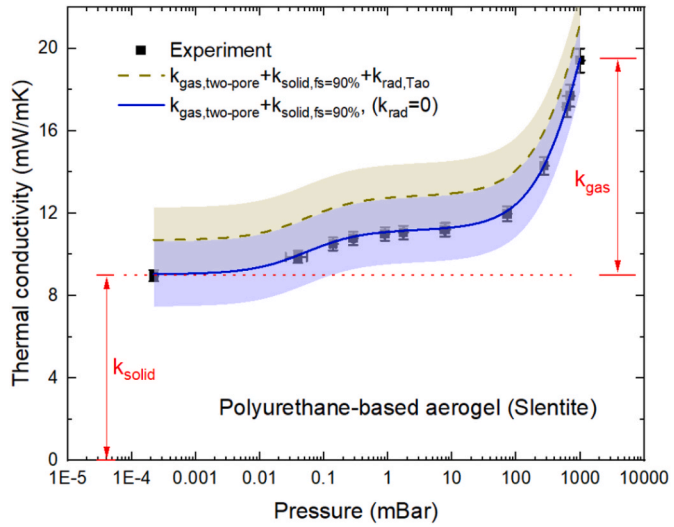

Fig. 11. The model prediction of $k_{gas} + k_{solid} + k_{rad}$ as compared with experimental data k_{eff} for PUR-based aerogel filled with air at 297 K as a function of pressure. Curves are theoretical predictions with different radiation models. The shaded area indicates the prediction uncertainty. This sample has a porosity of 89.5%, and a density of 0.1235 g/cm^3.

other polymers with smaller intrinsic k_s^0, such as polystyrene. For these materials, changing air to CO_2 (or other gases with lower thermal conductivity) may further reduce k_{eff} because CO_2 has a lower thermal conductivity than air and CO_2 MFP is larger than air. The gas with lower MFP benefits more from the small pore size. Since particulate aerogels have smaller gas accommodation coefficients, they might more easily achieve lower thermal conductivity values than foams. In addition, particulate aerogels can be made with engineered interfaces to further reduce thermal conductivity through a solid.

6.5. Coupling between solid, gas, and radiative conduction

As has been reported and studied in many works [48,53,54,65], the pressure-dependent thermal conductivity of some granular or

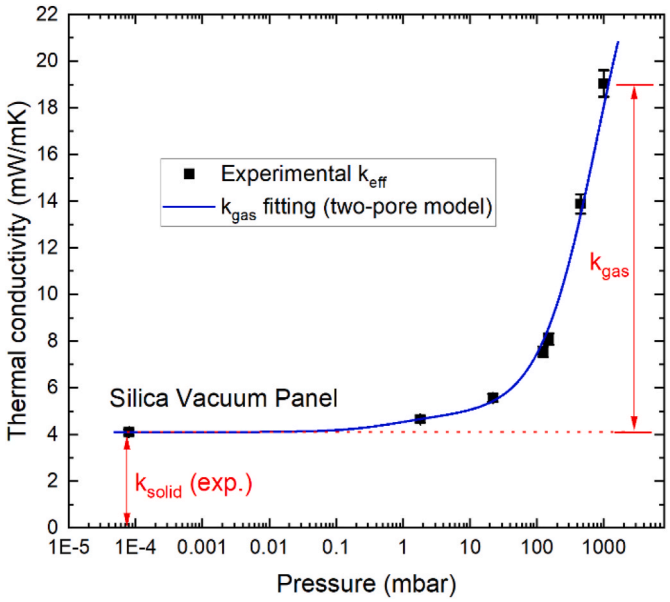

Fig. 12. The model prediction of $k_{gas} + k_{solid} + k_{rad}$ as compared with experimental data k_{eff} for fumed silica VIP core filled with air at 297 K as a function of pressure. The inset shows the solid thermal conductivity predicted by various models as compared with the experiment. This sample has a porosity of 91.08% and a density of 0.1962 g/cm^3.

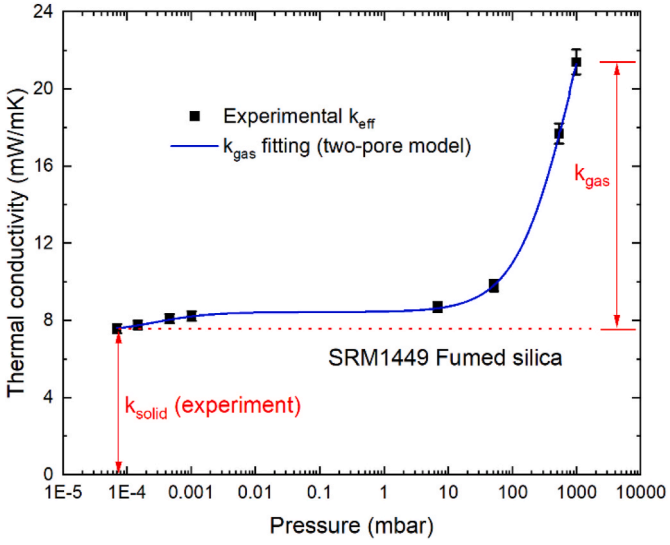

Fig. 13. The model prediction of $k_{gas} + k_{solid} + k_{rad}$ as compared to experimental data k_{eff} for SRM 1449 fumed silica filled with air at 297 K as a function of pressure. The inset shows the solid thermal conductivity predicted by various models as compared to the experiment. This sample has a porosity of 88.2% and a density of 0.331 g/cm^3.

fiber-based materials can exceed the theoretical maximum gaseous thermal conductivity. In our work, we also observed this phenomenon in glass fibers used in VIP cores, SRM 1450b fibrous-glass board, and calcium silicate. This abnormal pressure-dependent thermal conductivity has been reported as the coupling between gas thermal conductivity and solid thermal conductivity. When pressure is relatively high (e.g., >0.1 mbar), the solid can absorb some gases molecules, which can considerably increase the heat transport through the solid (k_{solid}). When pressure is low (e.g., vacuum), there are fewer gas molecules to be absorbed by the solid surfaces, and the solid heat transfer is reduced. Therefore, the effective thermal conductivity should be written as

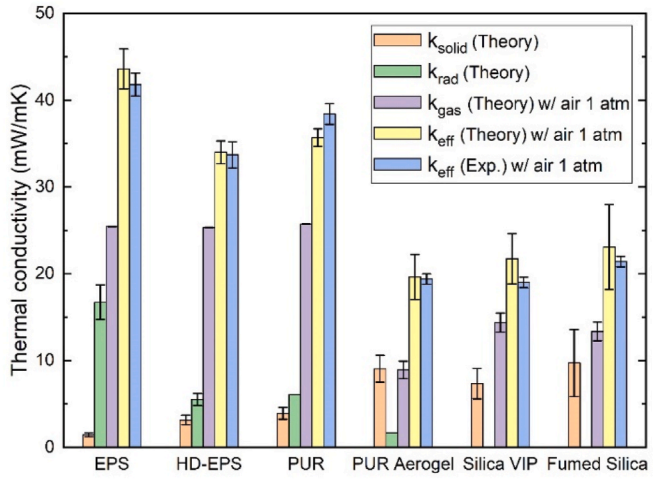

Fig. 14. The thermal conductivity components, k_{gas}, k_{solid}, k_{rad}, and the total effective thermal conductivity k_{eff} calculated from theories as compared with k_{eff} measured in our experiments. The data are for samples filled with air at 297 K, 1 atm.

$$k_{eff}(T,P) = k_{gas}(T,P) + k_{solid}(T) + k_{coupling}(T,P) + k_{rad}(T) \quad (33)$$

6.6. Near-field radiation

The other potentially important heat transfer mechanism is near-field radiation, which has been recently found to be important theoretically in polymer insulation foams when the pore size is below 1 μm [115]. Near-field radiation occurs at sub-wavelength separation distances when propagating electromagnetic waves experience interference and may exceed the blackbody limit by ~100 times owing to the tunneling of evanescent electromagnetic waves [116–118]. However, based on the radiative thermal conductance between two parallel SiO_2 plates measured in Ref. [118], the derived radiative thermal conductivity is only on the order of 0.01–0.1 mW m^{-1} K^{-1}, which is negligible compared with gas or solid thermal conductivity (See Fig. 15). The negligible radiative thermal conductivity can partially explain why VIPs can achieve ultrahigh R values. Nevertheless, the role of near-field

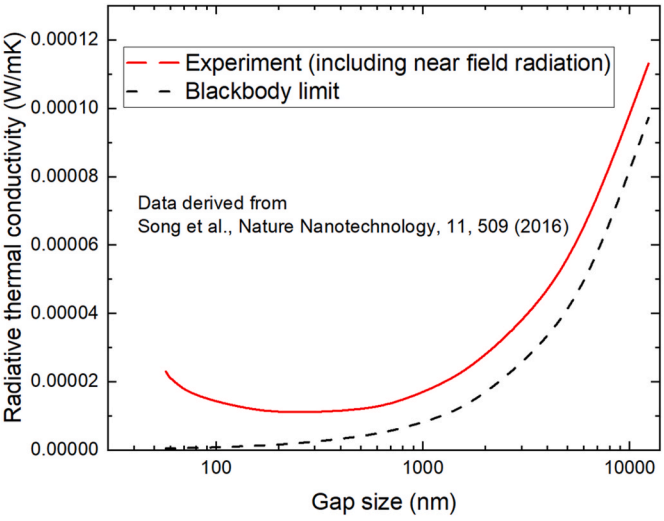

Fig. 15. Experimentally measured radiative thermal conductivity between two SiO_2 parallel plates at room temperature derived from the radiative thermal conductance G measured in Ref. [118] by using $k_{rad} = \frac{G}{A}d$, where A is the plates' area and d is the gap size.

radiation in thermal insulation materials is still open to investigation.

7. Conclusions

In this work, we improve the solid and gas thermal conductivity models to predict heat transfer through solid and gas in porous thermal insulation material. The former is realized by including the sound velocity softening in the EMA, and the latter is done by using the EMA model. Both improvements are crucial to calculate effective thermal conductivity of insulation materials. We decomposed gas, solid, and radiative thermal conductivities in several thermal insulation materials in EPS, HD-EPS and PUR foams, PUR aerogel, silica VIP, and fumed silica. For polymer foams (EPS, HD-EPS, and PUR in this work), k_{gas} and k_{rad} dominate the thermal conductivity whereas k_{solid} is very small, indicating that the most efficient way to reduce the effective thermal conductivity of cellular polymer foams is to reduce the pore size, which can simultaneously reduce k_{gas} and k_{rad}. For aerogels (PUR aerogel, silica VIP, and fumed silica), the dominant thermal conductivity components are k_{gas} and k_{solid} whereas k_{rad} is negligible owing to the small pore size and the addition of opacifiers, indicating that the most efficient ways to reduce k_{eff} are to further reduce pore size and to choose a solid material with low thermal conductivity k_s^0. This study is expected to provide guidance to the design and optimization of the next generation of thermal insulation materials for a broad scope of applications.

Additional notes

This paper has been authored by UT-Battelle, LLC, under contract DE-AC05-00OR22725 with the US Department of Energy (DOE). The US Government retains and the publisher, by accepting the article for publication, acknowledges that the US government retains a nonexclusive, paid-up, irrevocable, worldwide license to publish or reproduce the published form of this manuscript, or allow others to do so, for US government purposes. DOE will provide public access to these results of federally sponsored research in accordance with the DOE Public Access Plan (http://energy.gov/downloads/doe-public-access-plan).

Declaration of competing interest

The authors declare that they have no known competing financial interests or personal relationships that could have appeared to influence the work reported in this paper.

Data availability

Data will be made available on request.

Acknowledgments

This research was supported by the US Department of Energy's (DOE's) Office of Energy Efficiency and Renewable Energy (EERE), Building Technologies Office (BTO) under Contract No. DE-AC05-00OR22725 with UT-Battelle, LLC, and used resources at the Building Technologies and Research Integration Center, a DOE-EERE User Facility at Oak Ridge National Laboratory. The authors are grateful for the discussion with Alan McGaughey from Carnegie Mellon University. This work is supported by the project "Models to Evaluate and Guide the Development of Low Thermal Conductivity Materials for Building Envelopes" funded by the DOE's BTO and EERE. M.F. acknowledges the financial support from the National Science Foundation (grant CBET-1952210). The authors acknowledge the support from NanoPore Incorporated, National Institute of Standards and Technology, and BASF Corporation for providing samples used in this research. The authors also acknowledge the support from Jerry Atchley for preparing the samples and running experiments, Anthony Gehl for developing the DAQ for experimental setup, and Jaswinder Sharma, Kai Li, Qianying Guo, and Kinga Unocic for their help with conducting SEM measurements. The authors thank Olivia Shafer for formatting and technical editing.

Appendix A. Supplementary data

Supplementary data to this article can be found online at https://doi.org/10.1016/j.ijthermalsci.2023.108164.

References

[1] M.S. Al-Homoud, Performance characteristics and practical applications of common building thermal insulation materials, Build. Environ. 40 (2005) 353.
[2] B.P. Jelle, A. Gustavsen, R. Baetens, The path to the high performance thermal building insulation materials and solutions of tomorrow, J. Build. Phys. 34 (2010) 99.
[3] A.M. Papadopoulos, E. Giama, Environmental performance evaluation of thermal insulation materials and its impact on the building, Build. Environ. 42 (2007) 2178.
[4] A. M. A.-T. G. M. Zaki, Optimization of multilayer thermal insulation for pipelines, Heat Tran. Eng. 21 (2000) 63.
[5] D. Glass, Ceramic matrix composite (CMC) thermal protection systems (TPS) and hot structures for hypersonic vehicles, in: 15th AIAA International Space Planes and Hypersonic Systems and Technologies Conference, American Institute of Aeronautics and Astronautics, Reston, Virginia, 2008.
[6] Y. Bao, X. Zhao, The research applications of new heat insulation composite material in automobiles, Heat Tran. Asian Res. 47 (2018) 103.
[7] J.S. Lim, A. Bejan, Two fundamental problems of refrigerator thermal insulation design, Heat Tran. Eng. 15 (1994) 35.
[8] A. Oushabi, S. Sair, Y. Abboud, O. Tanane, A. El Bouari, Natural thermal-insulation materials composed of renewable resources: characterization of local date palm fibers (LDPF), J. Mater. Environ. Sci. 6 (2015) 3395.
[9] U. Kartoglu, J. Milstien, Tools and approaches to ensure quality of vaccines throughout the cold chain, Expert Rev. Vaccines 13 (2014) 843.
[10] U. S., Energy Information Administration/Monthly Energy Review March 2020 (2020) 37.
[11] A.G. Gaglia, E.N. Dialynas, A.A. Argiriou, E. Kostopoulou, D. Tsiamitros, D. Stimoniaris, K.M. Laskos, Energy performance of European residential buildings: energy use, technical and environmental characteristics of the Greek residential sector – energy conservation and CO_2 reduction, Energy Build. 183 (2019) 86.
[12] K. Sawyer, Windows and Building Envelope Research and Development, Roadmap for Emerging Technologies, 2014.
[13] M. Kaviany, Principles of Heat Transfer in Porous Media, Springer Science \& Business Media, 2012.
[14] B. Notario, J. Pinto, E. Solorzano, J.A. De Saja, M. Dumon, M.A. Rodríguez-Pérez, Experimental validation of the knudsen effect in nanocellular polymeric foams, Polymer 56 (2015) 57.
[15] H. Rezgar, A. Taher, D. Ali, E.L. Richard, Thermal conductivity of low density polyethylene foams Part I: comprehensive study of theoretical models, J. Therm. Sci. 28 (2019) 745.
[16] H. Zhang, W. Fang, Z. Li, W. Tao, The influence of gaseous heat conduction to the effective thermal conductivity of nano-porous materials, Int. Commun. Heat Mass Tran. 68 (2015) 158.
[17] D. Dan, H. Zhang, W.-Q. Tao, Effective structure of aerogels and decomposed contributions of its thermal conductivity, Appl. Therm. Eng. 72 (2014) 2.
[18] W. Van De Walle, Prediction of the Effective Thermal Conductivity of Porous Building Blocks Based on Their Pore Structure, 2019.
[19] F. Hu, S. Wu, Y. Sun, Hollow-structured materials for thermal insulation, Adv. Mater. 31 (2019), 1801001.
[20] Y.J. Dai, Y.Q. Tang, W.Z. Fang, H. Zhang, W.Q. Tao, A theoretical model for the effective thermal conductivity of silica aerogel composites, Appl. Therm. Eng. 128 (2018) 1634.
[21] Y. Liang, Y. Ding, Y. Liu, J. Yang, H. Zhang, Modeling microstructure effect on thermal conductivity of aerogel-based vacuum insulation panels, Heat Tran. Eng. 41 (2020) 882.
[22] Y. Liang, H. Wu, G. Huang, J. Yang, Y. Ding, Prediction and optimization of thermal conductivity of vacuum insulation panels with aerogel composite cores, Procedia Eng. 205 (2017) 2855.
[23] B.P. Jelle, Nano-Based Thermal Insulation for Energy-Efficient Buildings, Elsevier Ltd, 2016.
[24] G.H. Tang, C. Bi, Y. Zhao, W.Q. Tao, Thermal transport in nano-porous insulation of aerogel: factors, models and outlook, Energy 90 (2015) 701.
[25] S. Liu, J. Duvigneau, G.J. Vancso, Nanocellular polymer foams as promising high performance thermal insulation materials, Eur. Polym. J. 65 (2015) 33.
[26] Y.L. He, T. Xie, Advances of thermal conductivity models of nanoscale silica aerogel insulation material, Appl. Therm. Eng. 81 (2015) 28.
[27] S. Kang, J. Choi, S. Choi, Mechanism of heat transfer through porous media of inorganic intumescent coating in cone calorimeter testing, Polymers 11 (2019) 221.

[28] S. Shrestha, A. Rai, T. Feng, M. Zhang, D.E. Hun, K. Biswas, A.O. Desjarlais, Review of models to evaluate and Guide the development of low-thermal-conductivity materials, in: Thermal Performance of the Exterior Envelopes of Whole Buildings XIV International Conference, 2019, p. 67.
[29] Z. Jia, Z. Wang, D. Hwang, L. Wang, Prediction of the effective thermal conductivity of hollow sphere foams, ACS Appl. Energy Mater. 1 (2018) 1146.
[30] S. Azeem, M. Zain-Ul-Abdein, Investigation of thermal conductivity enhancement in bakelite-graphite particulate filled polymeric composite, Int. J. Eng. Sci. 52 (2012) 30.
[31] R.C. Progelhof, J.L. Throne, R.R. Ruetsch, Methods for predicting the thermal conductivity of composite systems: a review, Polym. Eng. Sci. 16 (1976) 615.
[32] H.W. Russell, Principles of heat flow in porous insulators, J. Am. Ceram. Soc. 18 (1935) 1.
[33] J.C. Maxwell, A Treatise on Electricity and Magnetism, vol. 1, Clarendon press, 1881.
[34] V.A. Markel, Introduction to the Maxwell garnett approximation: tutorial, J. Opt. Soc. Am. 33 (2016) 1244.
[35] A. Eucken, Allgemeine gesetzmäßigkeiten für das wärmeleitvermögen verschiedener stoffarten und aggregatzustände, Forschung Auf Dem Gebiet Des Ingenieurwesens A 11 (1940) 6.
[36] N.C. Hilyard, A. Cunningham, Low Density Cellular Plastics, Springer Netherlands, Dordrecht, 1994.
[37] T. Bauer, A general analytical approach toward the thermal conductivity of porous media, Int. J. Heat Mass Tran. 36 (1993) 4181.
[38] J.D. Moreno, Radiative Transfer and Thermal Performance Levels in Foam Insulation Boardstocks, 1991.
[39] L.R. Glicksman, M. Torpey, Factors governing heat transfer through closed cell foam insulation, J. Therm. Insul. 12 (1989) 257.
[40] M. Kashiwagi, Y. Sudo, T. Shiga, J. Shiomi, Modeling heat conduction in nanoporous silicon with geometry distributions, Phys Rev Appl 10 (2018), 044018.
[41] E.E. Gonzo, Estimating correlations for the effective thermal conductivity of granular materials, Chem. Eng. J. 90 (2002) 299.
[42] A. Rai, T. Feng, D. Howard, D. Hun, M. Zhang, H. Zhou, S.S. Shrestha, Conduction heat transfer through solid in porous materials: a comparative study by finite-element simulations and effective medium approximations, Comput. Therm. Sci. 13 (2021) 19.
[43] J. Gross, J. Fricke, Ultrasonic velocity measurements in silica, carbon and organic aerogels, J. Non-Cryst. Solids 145 (1992) 217.
[44] O. Nilsson, G. Rueschenpoehler, J. Gross, J. Fricke, Correlation between Thermal Conductivity and Elasto-Mechanical Properties of Compressed Porous Media, vol. 21, High Temp High Press, 1989, p. 267.
[45] O.J. Lee, K.H. Lee, T. Jin Yim, S. Young Kim, K.P. Yoo, Determination of mesopore size of aerogels from thermal conductivity measurements, J. Non-Cryst. Solids 298 (2002) 287.
[46] W.P. Hsieh, M.D. Losego, P.V. Braun, S. Shenogin, P. Keblinski, D.G. Cahill, Testing the minimum thermal conductivity model for amorphous polymers using high pressure, Phys. Rev. B Condens. Matter 83 (2011), 174205.
[47] X. Xie, D. Li, T.H. Tsai, J. Liu, P.V. Braun, D.G. Cahill, Thermal conductivity, heat capacity, and elastic constants of water-soluble polymers and polymer blends, Macromolecules 49 (2016) 972.
[48] C. Bi, G.H. Tang, Z.J. Hu, H.L. Yang, J.N. Li, Coupling model for heat transfer between solid and gas phases in aerogel and experimental investigation, Int. J. Heat Mass Tran. 79 (2014) 126.
[49] J. Gross, J. Fricke, L.W. Hrubesh, Sound propagation in SiO2 aerogels, J. Acoust. Soc. Am. 91 (1992) 2004.
[50] V. Nemanič, B. Zajec, M. Žumer, N. Figar, M. Kavšek, I. Mihelič, Synthesis and characterization of melamine-formaldehyde rigid foams for vacuum thermal insulation, Appl. Energy 114 (2014) 320.
[51] K. Raed, U. Gross, Modeling of influence of gas atmosphere and pore-size distribution on the effective thermal conductivity of knudsen and non-knudsen porous materials, Int. J. Thermophys. 30 (2009) 1343.
[52] P. Gong, P. Buahom, M.P. Tran, M. Saniei, C.B. Park, P. Pötschke, Heat transfer in microcellular polystyrene/multi-walled carbon nanotube nanocomposite foams, Carbon N Y 93 (2015) 819.
[53] J.J. Zhao, Y.Y. Duan, X.D. Wang, B.X. Wang, Effects of solid-gas coupling and pore and particle microstructures on the effective gaseous thermal conductivity in aerogels, J. Nanoparticle Res. 14 (2012) 1024.
[54] K. Swimm, G. Reichenauer, S. Vidi, H.P. Ebert, Impact of thermal coupling effects on the effective thermal conductivity of aerogels, J. Sol. Gel Sci. Technol. 84 (2017) 466.
[55] M. Wiener, G. Reichenauer, S. Braxmeier, F. Hemberger, H.P. Ebert, Carbon aerogel-based high-temperature thermal insulation, Int. J. Thermophys. 30 (2009) 1372.
[56] G. Reichenauer, U. Heinemann, H.P. Ebert, Relationship between pore size and the gas pressure dependence of the gaseous thermal conductivity, Colloids Surf. A Physicochem. Eng. Asp. 300 (2007) 204.
[57] C. Bi, G.H. Tang, W.Q. Tao, Prediction of the gaseous thermal conductivity in aerogels with non-uniform pore-size distribution, J. Non-Cryst. Solids 358 (2012) 3124.
[58] Z.Y. Li, C.Y. Zhu, X.P. Zhao, A theoretical and numerical study on the gas-contributed thermal conductivity in aerogel, Int. J. Heat Mass Tran. 108 (2017) 1982.
[59] M. Bouquerel, T. Duforestel, D. Baillis, G. Rusaouen, Heat transfer modeling in vacuum insulation panels containing nanoporous silicas - a review, Energy Build. 54 (2012) 320.
[60] F.O. Goodman, Thermal accommodation coefficients, J. Phys. Chem. 84 (1980) 1431.
[61] T.M. Flynn, Cryogenic Engineering, second ed., Marcel Dekker, New York, NY 10016, U.S.A., 2005. Revised and Expanded.
[62] T. Feng, A. Rai, D. Hun, S.S. Shrestha, Molecular dynamics simulations of energy accommodation between gases and polymers for ultra-low thermal conductivity insulation, Int. J. Heat Mass Tran. 164 (2021), 120459.
[63] M.G. Kaganer, *Thermal Insulation In Cryogenic Engineering* (Jerusalem, Israel Program for Scientific Translations, 1969.
[64] B. Gebhart, Heat Conduction and Mass Diffusion, McGraw-Hill, New York, 1993.
[65] K. Swimm, S. Vidi, G. Reichenauer, H.P. Ebert, Coupling of gaseous and solid thermal conduction in porous solids, J. Non-Cryst. Solids 456 (2017) 114.
[66] R. Coquard, D. Baillis, V. Grigorova, F. Enguehard, D. Quenard, P. Levitz, Modelling of the conductive heat transfer through nano-structured porous silica materials, J. Non-Cryst. Solids 363 (2013) 103.
[67] W.J. Batty, S.D. Probert, P.W. O'Callaghan, Apparent thermal conductivities of high-porosity cellular insulants, Appl. Energy 18 (1984) 117.
[68] M.A. Schuetz, L.R. Glicksman, A basic study of heat transfer through foam insulation, J. Cell. Plast. 20 (1984) 114.
[69] R.J.J. Williams, C.M. Aldao, Thermal conductivity of plastic foams, Polym. Eng. Sci. 23 (1983) 293.
[70] J. Kuhn, H.P. Ebert, M.C. Arduini-Schuster, D. Büttner, J. Fricke, Thermal transport in polystyrene and polyurethane foam insulations, Int. J. Heat Mass Tran. 35 (1992) 1795.
[71] E. Placido, M.C. Arduini-Schuster, J. Kuhn, Thermal properties predictive model for insulating foams, Infrared Phys. Technol. 46 (2005) 219.
[72] P. Hsu, J.R. Howell, Measurements of thermal conductivity and optical properties of porous partially stabilized zirconia, Exp. Heat Tran. 5 (1992) 293.
[73] T.J. Hendricks, J.R. Howell, Absorption/scattering coefficients and scattering phase functions in reticulated porous ceramics, J. Heat Tran. 118 (1996) 79.
[74] W.-H. Tao, H.-C. Hsu, C.-C. Chang, C.-L. Hsu, Y.-S. Lin, Measurement and prediction of thermal conductivity of open cell rigid polyurethane foam, J. Cell. Plast. 37 (2001) 310.
[75] O.A. Almanza, M.A. Rodríguez-Pérez, J.A. De Saja, Prediction of the radiation term in the thermal conductivity of crosslinked closed cell polyolefin foams, J. Polym. Sci. B Polym. Phys. 38 (2000) 993.
[76] E. Solórzano, M.A. Rodriguez-Perez, J. Lazaro, J.A. De Saja, Influence of solid phase conductivity and cellular structure on the heat transfer mechanisms of cellular materials: diverse case studies, Adv. Eng. Mater. 11 (2009) 818.
[77] M.A. Rodríguez-Pérez, J.I. González-Peña, N. Witten, J.A. de Saja, The effect of cell size on the physical properties of crosslinked closed cell polyethylene foams produced by a high pressure nitrogen solution process, Cell. Polym. 21 (2002) 165.
[78] J.A. Martínez-Díez, M.A. Rodríguez-Pérez, J.A. De Saja, L.O. Arcos Y Rábago, O. A. Almanza, The thermal conductivity of a polyethylene foam block produced by a compression molding process, J. Cell. Plast. 37 (2001) 21.
[79] C. De Micco, C.M. Aldao, Radiation contribution to the thermal conductivity of plastic foams, J. Polym. Sci. B Polym. Phys. 43 (2005) 190.
[80] X.D. Wang, D. Sun, Y.Y. Duan, Z.J. Hu, Radiative characteristics of opacifier-loaded silica aerogel composites, J. Non-Cryst. Solids 375 (2013) 31.
[81] C.F. Bohren, D.R. Huffman, Absorption and Scattering of Light by Small Particles, John Wiley & Sons, 2008.
[82] F. Wang, J. Tan, S. Yong, H. Tan, S. Chu, Thermal performance analyses of porous media solar receiver with different irradiative transfer models, Int. J. Heat Mass Tran. 78 (2014) 7.
[83] J.R. Howell, M.J. Hall, J.L. Ellzey, Combustion of hydrocarbon fuels within porous inert media, Prog. Energy Combust. Sci. 22 (1996) 121.
[84] Z. Wu, C. Caliot, G. Flamant, Z. Wang, Coupled radiation and flow modeling in ceramic foam volumetric solar air receivers, Sol. Energy 85 (2011) 2374.
[85] M.A. Mujeebu, M.Z. Abdullah, A.A. Mohamad, M.Z.A. Bakar, Trends in modeling of porous media combustion, Prog. Energy Combust. Sci. 36 (2010) 627.
[86] R. Mital, J.P. Gore, R. Viskanta, Measurements of radiative properties of cellular ceramics at high temperatures, J. Thermophys. Heat Tran. 10 (1996) 33.
[87] H.B. Gao, Z.G. Qu, X.B. Feng, W.Q. Tao, Methane/air premixed combustion in a two-layer porous burner with different foam materials, Fuel 115 (2014) 154.
[88] L. Aichmayer, J. Spelling, B. Laumert, Preliminary design and analysis of a novel solar receiver for a micro gas-turbine based solar dish system, Sol. Energy 114 (2015) 378.
[89] S. Haussener, A. Steinfeld, Effective heat and mass transport properties of anisotropic porous ceria for solar thermochemical fuel generation, Materials 5 (2012) 192.
[90] S. Cunsolo, R. Coquard, D. Baillis, W.K.S. Chiu, N. Bianco, Radiative properties of irregular open cell solid foams, Int. J. Therm. Sci. 117 (2017) 77.
[91] Y. Li, X.L. Xia, C. Sun, S. De Zhang, H.P. Tan, Volumetric radiative properties of irregular open-cell foams made from semitransparent absorbing-scattering media, J. Quant. Spectrosc. Radiat. Transf. 224 (2019) 325.
[92] M. Loretz, E. Maire, D. Baillis, Analytical modelling of the radiative properties of metallic foams: contribution of X-ray tomography, Adv. Eng. Mater. 10 (2008) 352.
[93] R.A. Campo-Arnáiz, M.A. Rodríguez-Pérez, B. Calvo, J.A. De Saja, Extinction coefficient of polyolefin foams, J. Polym. Sci. B Polym. Phys. 43 (2005) 1608.
[94] A. Kaemmerlen, C. Vo, F. Asllanaj, G. Jeandel, D. Baillis, Radiative properties of extruded polystyrene foams: predictive model and experimental results, J. Quant. Spectrosc. Radiat. Transf. 111 (2010) 865.
[95] M. Santiago-Calvo, J. Tirado-Mediavilla, J.L. Ruiz-Herrero, F. Villafañe, M.Á. Rodríguez-Pérez, Long-term thermal conductivity of cyclopentane–water

blown rigid polyurethane foams reinforced with different types of fillers, Polym. Int. 68 (2019) 1826.
[96] L.R. Glicksman, Heat transfer and ageing of cellular foam insulation, Cell. Polym. 10 (1991) 276.
[97] M. Wang, N. Pan, Predictions of effective physical properties of complex multiphase materials, Mater. Sci. Eng. R Rep. 63 (2008) 1.
[98] M. Wang, N. Pan, Modeling and prediction of the effective thermal conductivity of random open-cell porous foams, Int. J. Heat Mass Tran. 51 (2008) 1325.
[99] J.S. Kwon, C.H. Jang, H. Jung, T.H. Song, Effective thermal conductivity of various filling materials for vacuum insulation panels, Int. J. Heat Mass Tran. 52 (2009) 5525.
[100] E.N. Schmierer, A. Razani, Self-consistent open-celled metal foam model for thermal applications, J. Heat Tran. 128 (2006) 1194.
[101] V.S. Shabde, K.A. Hoo, G.M. Gladysz, Experimental determination of the thermal conductivity of three-phase syntactic foams, J. Mater. Sci. 41 (2006) 4061.
[102] C. Bi, G. Tang, Q. Sheng, B. Fu, Study on thermal conductivity of gas phase in nano-porous aerogel, 4th Micro and Nano Flows Conference (2014).
[103] ASTM Int, C518-15: Standard Test Method for Steady-State Thermal Transmission Properties by Means of the Heat Flow Meter Apparatus, vol. 1, ASTM International, 2015.
[104] M.C. Wingert, J. Zheng, S. Kwon, R. Chen, Thermal transport in amorphous materials: a review, Semicond. Sci. Technol. 31 (2016), 113003.
[105] K. Swimm, G. Reichenauer, S. Vidi, H.-P. Ebert, Gas pressure dependence of the heat transport in porous solids with pores smaller than 10 μm, Int. J. Thermophys. 30 (2009) 1329.
[106] J.C. Harper, A.F. El Sahrigi, Thermal conductivities of gas-filled porous solids, Ind. Eng. Chem. Fundam. 3 (1964) 318.
[107] S.Q. Zeng, A.J. Hunt, W. Cao, R. Greif, Pore size distribution and apparent gas thermal conductivity of silica aerogel, J. Heat Tran. 116 (1994) 756.
[108] S.Q. Zeng, A. Hunt, R. Greif, Mean free path and apparent thermal conductivity of a gas in a porous medium, J. Heat Tran. 117 (1995) 758.
[109] G. Wei, Y. Liu, X. Zhang, F. Yu, X. Du, Thermal conductivities study on silica aerogel and its composite insulation materials, Int. J. Heat Mass Tran. 54 (2011) 2355.
[110] M. Biron, Detailed accounts of thermoplastic resins, in: Thermoplastics and Thermoplastic Composites, Elsevier, 2013, pp. 189–714.
[111] L.V. Nielsen, H.P. Ebert, F. Hemberger, J. Fricke, A. Biedermann, M. Reichelt, U. Rotermund, Thermal Conductivity of Nonporous Polyurethane, vol. 32, High Temp High Press, 2000, p. 701.
[112] S.C. Kim, D. Klempner, K.C. Frisch, H.L. Frisch, Polyurethane interpenetrating polymer networks. II. Density and glass transition behavior of polyurethane-poly (methyl methacrylate) and polyurethane-polystyrene IPN'S, Macromolecules 9 (1976) 263.
[113] F. Saint-Michel, L. Chazeau, J.Y. Cavaillé, E. Chabert, Mechanical properties of high density polyurethane foams: I. Effect of the density, Compos. Sci. Technol. 66 (2006) 2700.
[114] P. Singhal, J.N. Rodriguez, W. Small, S. Eagleston, J. Van De Water, D. J. Maitland, T.S. Wilson, Ultra low density and highly crosslinked biocompatible shape memory polyurethane foams, J. Polym. Sci. B Polym. Phys. 50 (2012) 724.
[115] P. Buahom, C. Wang, M. Alshrah, G. Wang, P. Gong, M.P. Tran, C.B. Park, Wrong expectation of superinsulation behavior from largely-expanded nanocellular foams, Nanoscale 12 (2020), 13064.
[116] K. Joulain, J.P. Mulet, F. Marquier, R. Carminati, J.J. Greffet, Surface electromagnetic waves thermally excited: radiative heat transfer, coherence properties and casimir forces revisited in the near field, Surf. Sci. Rep. 57 (2005) 59.
[117] M. Francoeur, Near-field thermal radiation, in: F. Kulacki (Ed.), Handbook of Thermal Science and Engineering, Springer, Cham, 2017, pp. 1–43.
[118] B. Song, D. Thompson, A. Fiorino, Y. Ganjeh, P. Reddy, E. Meyhofer, Radiative heat conductances between dielectric and metallic parallel plates with nanoscale gaps, Nat. Nanotechnol. 11 (2016) 509.